

# Modeling drifter trajectories and ensemble dispersion from the Ocean Training Course 2025

Samantha Kucher

Vadim Bertrand

## Table of contents

<b>1</b>	<b>Introduction</b>	<b>1</b>
<b>2</b>	<b>Instruments, data and methods</b>	<b>2</b>
2.1	Drifters deployed during the campaign . . . . .	2
2.1.1	MELODI . . . . .	2
2.1.2	SPOT . . . . .	4
2.2	Satellite and drifter data . . . . .	6
2.2.1	Satellite-derived gridded products . . . . .	6
2.2.2	Drifter data . . . . .	7
2.3	Modeling of drifter trajectories . . . . .	9
2.3.1	Linear combination . . . . .	9
2.3.2	Maxey-Riley framework . . . . .	9
2.4	Pair dispersion . . . . .	10
<b>3</b>	<b>Results</b>	<b>11</b>
3.1	Modeling of drifter trajectories . . . . .	11
3.1.1	Maxey-Riley framework . . . . .	11
3.2	Pair dispersion . . . . .	11
<b>4</b>	<b>Discussion</b>	<b>16</b>
4.1	Modeling of drifter trajectories . . . . .	16
4.1.1	Maxey-Riley framework . . . . .	16
4.2	Pair dispersion . . . . .	17
<b>5</b>	<b>Conclusion</b>	<b>18</b>
<b>6</b>	<b>Acknowledgements</b>	<b>18</b>

## 1 Introduction

Better understanding of particle transport in the ocean is crucial to reduce marine plastic pollution. The life of microplastics in the ocean is nonetheless complex: they can be transported through long distances by currents and gyres, mixed in turbulent flows, broken into smaller pieces, and sinked by biofouling ([Sutherland et al., 2023](#)). Recent laboratory experiments and theoretical developments have been made to study the influence of particle size, shape and density ([Clark et al., 2020](#)), ([DiBenedetto et al., 2022](#)), ([R. Calvert et al., 2024](#)). There is a growing interest in narrowing the gap between controlled experiments and real-world conditions found in the ocean.

Oceanic models are able to forecast the ocean state several days ahead, but they are not capable of resolving the small scales corresponding to particle transport. The combined effect of waves, currents and wind must be taken into account to predict the drift of passive tracers ([Christensen et al., 2018](#)). Parametrizing the

movement of particles in wavy, turbulent flows thus presents a fundamental challenge (Van Sebille et al., 2020), (Sutherland et al., 2023).

It has been shown that large non-Lagrangian floating particles experience a drift larger than the Stokes drift (Ross Calvert et al., 2021). This is due to the object oscillation relative to the free surface and its submergence, which changes continuously with the wave slope. The size of the object with respect to the wavelength is a determining factor in the drifting velocity. In the ocean, the dynamics of currents strongly impacts the propagation of wave fields (Quilfen & Chapron, 2019), and therefore modifies the particles trajectories. The impact of wind has also been addressed, using a leeway modeling approach to gain physical understanding of the forces that play a role in the drift of floating objects (Wagner et al., 2022). This model, however, does not accurately predict the trajectories of floating particles. Such prediction is given by the Maxey-Riley set for inertial surface particles Beron-Vera et al. (2019).

Satellite-tracked drifters have been studied in the North Atlantic (S. Elipot et al., 2016), and an *in-situ* study has been made in the Florida Current (Olascoaga et al., 2020). In the latter, the trajectory of buoys has been followed for one week. The authors successfully modeled the experimental data using a framework derived from the Maxey-Riley equations.

This project aims to reconstruct the trajectory of drifters deployed during the expedition and to better understand how physical processes govern their motion. We thus need to take into account the satellite measurements of sea surface deformation, wave induced currents and wind speed. We employ a two folded approach: (i) in first approximation a linear combination of the surface currents, Stokes drift and direct wind-force, and (ii) the full equations describing the dynamics of floating inertial particles in the ocean: the Maxey-Riley set. These two methods will allow us to decompose and analyze the individual forces governing the drifter's motion, providing deeper insights into the underlying dynamics.

We focus here on deterministic modellings of the drift. However, given the inherent chaotic nature of the problem and the uncertainties carried by our observations of oceanic and atmospheric variables, stochastic approaches might be relevant to simulate ensemble of probable and realistic trajectories, rather than one *incorrect* estimate. One challenge is to control the dispersion of simulated ensembles to accurately cover the distribution of possible trajectories. To address this question we study the relative dispersion over time of several ensembles of drifters deployed at the same space-time position.

## 2 Instruments, data and methods

This section describes the two types of drifters deployed during OTC25, as well as the data and trajectory reconstruction methods used in our analysis. We first present the design of the MELODI and SPOT drifters. Next, we introduce the different satellite-derived and drifter datasets (including the preprocessing steps applied when relevant). Finally, we detail the Lagrangian statistics used to characterize the drift dynamics, the trajectory reconstruction methods implemented, and the metrics employed to evaluate them.

### 2.1 Drifters deployed during the campaign

Figure 1 shows a photograph of all drifter types deployed during the campaign. At the time of writing, only eOdyn MELODI and IGE SPOT data are available, and we therefore focus on these two types. However, it should be noted that 16 OpenMetBuoy, 4 CLS MARGE-T II, and 1 Sofar Spotter buoy were also deployed. Including these additional drifters would strengthen our analysis, as we will discuss in Section 4.

#### 2.1.1 MELODI

The MELODI (“MELODI,” 2024) is a surface drifter developed by the company eOdyn. Although we are only interested in the drifter’s position, it also measures surface currents, surface temperature and wave parameters. The position is determined using several satellite constellations, with a sampling frequency of 1 hour. The drifter uses the Iridium satellite network to transmit its data. It is powered by four Li-ion 3500 mAh, 3.7 V batteries and a 6 W solar panel, which allows it to operate for at least several months. Thanks to its low-profile, see Figure 2, the MELODI drifter is expected to be only weakly affected by wind drift.

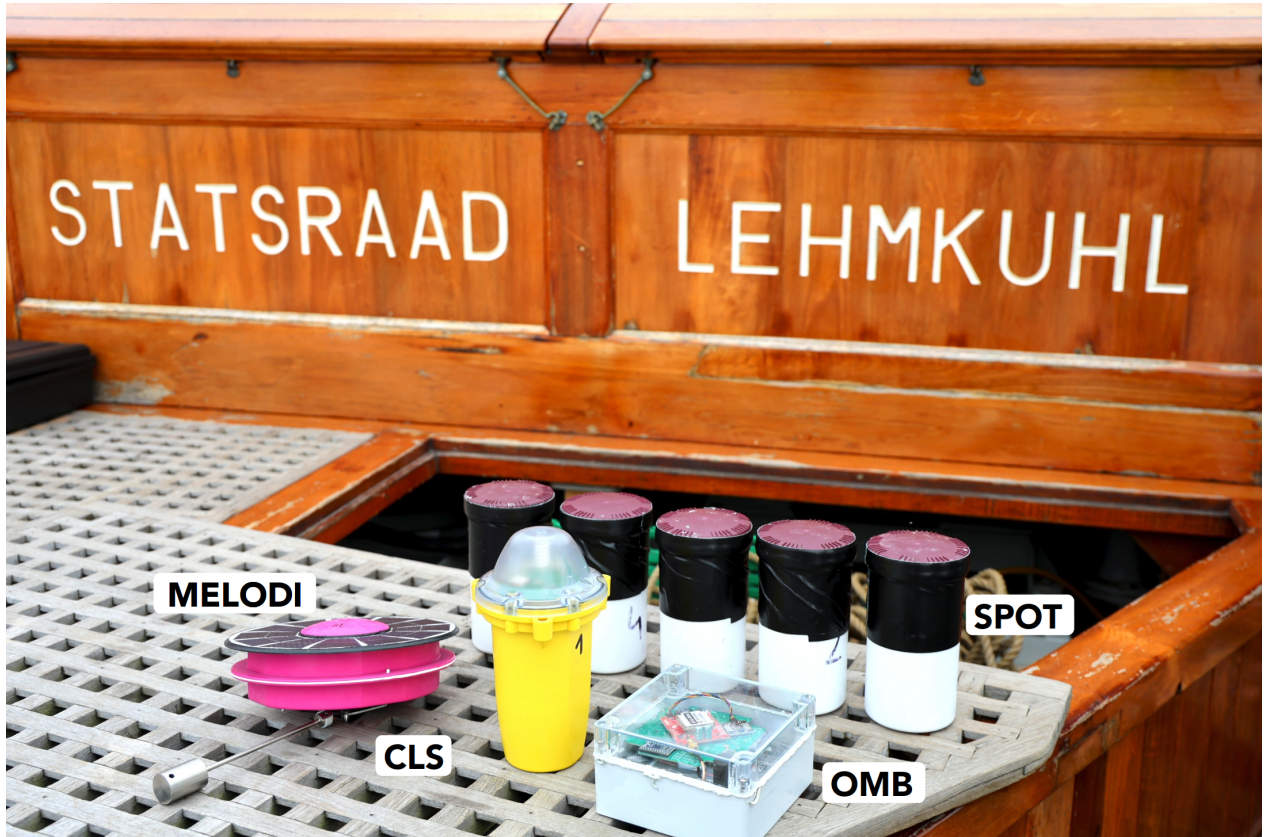


Figure 1: Types of drifters deployed during the OTC25 campaign between Tromsø and Nice. There was also a Sofar drifter not shown in the picture. Photo taken by Joël Marc.

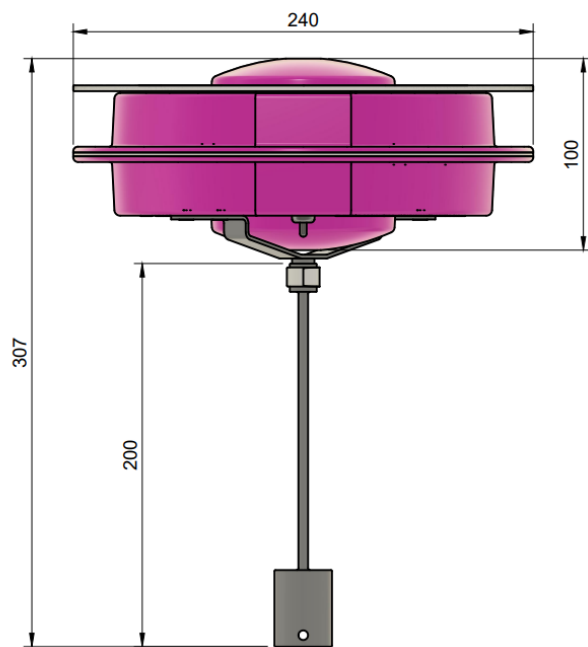


Figure 2: Design of the MELODI drifter

From Tromsø to Nice, 18 MELODI drifters were deployed in various locations: in the North Sea and its Lofoten eddy, in the North Atlantic (including during a storm event), before and after the Strait of Gibraltar (within the Alboran eddy), and in the western Mediterranean Sea. This can be seen in Figure 3.

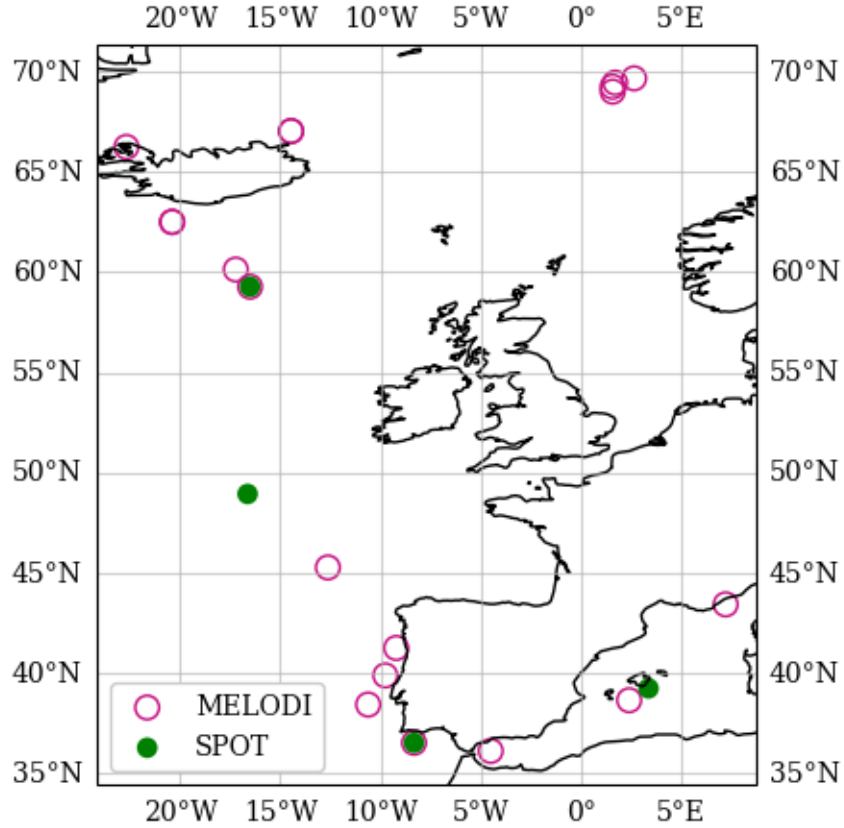


Figure 3: MELODI and SPOT drifter deployments during the OTC25 campaign.

### 2.1.2 SPOT

The SPOT (“[SPOT](#),” 2024) is a home-made surface drifter designed and developed at Institut des Géosciences de l’Environnement (IGE). Its design is very simple, see Figure 4: a weighted waterproof jar containing a GPS tracer powered by external batteries. The GPS tracer is a SPOT Trace, which uses the Globalstar satellite network to transmit its position every 30 minutes. External batteries (4 LR20 alkaline 1.5V 13Ah) allow the drifter to operate for up to 6 months and counting at the time of writing.

During the first deployments we noticed that the SPOT drifters exhibited an orbital motion around their vertical axis and we suspected that it was the cause for the observed effective sampling frequency being larger than the nominal 30 minutes (see Figure 6). To mitigate this motion we designed a dynamic anchor attached to the bottom of the drifter. Being at sea we had to reuse material available aboard the ship: old sails and steel wire ropes, as visible in Figure 5.

The last 5 drifters deployed in the Mediterranean Sea were equipped with this anchor. Using the drifter data presented in Section 2.2.2 it seems that the anchor was effective in improving the effective sampling frequency, as shown in Figure 6. Further analysis would be required to confirm this is due to the dynamic anchor and not because of an overall quieter sea state in the Mediterranean Sea.

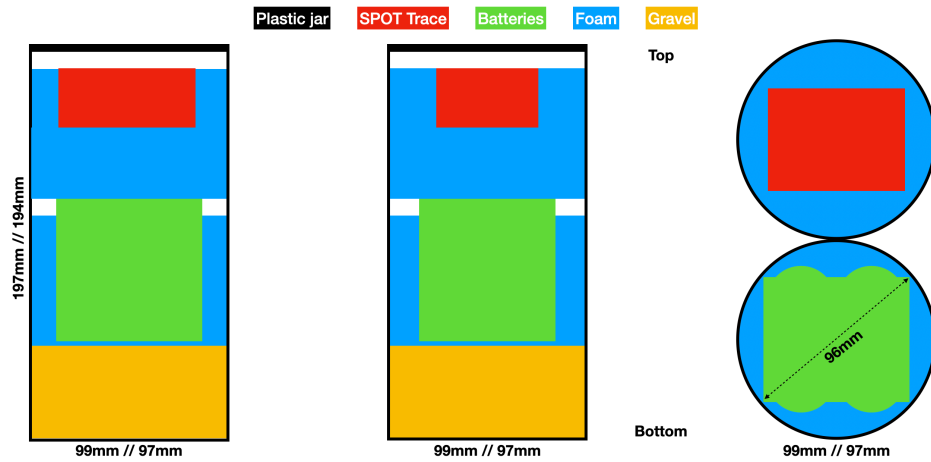


Figure 4: Design of the SPOT drifter



Figure 5: SPOT drifter with a dynamic anchor

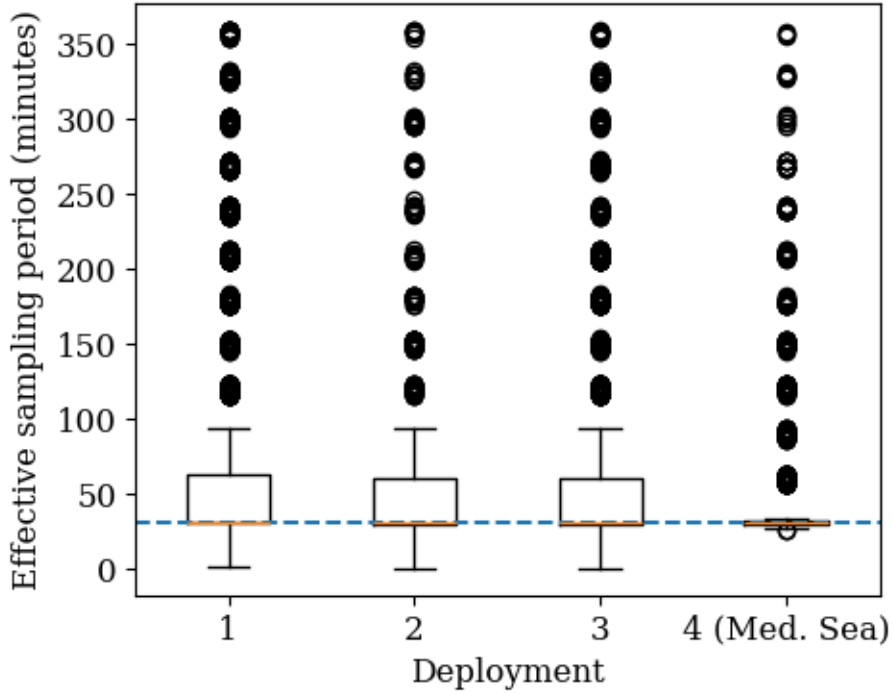


Figure 6: SPOT drifters effective sampling period. The dashed blue line indicates the nominal sampling period of 30 minutes.

Je pense que cette figure n'est pas si simple à interpréter parce que ça donne l'impression que les derniers drifters ont marché super bien, mais en vrai 1 était mort et 2 autres ont pas beaucoup transmis. Cette représentation prends pas en compte la quantité de drifters qui transmettent et pendant combien de temps ils ont vécu

## 2.2 Satellite and drifter data

Our analysis requires both maps of geophysical quantities (surface currents, waves, winds) and lagrangian drifter trajectories.

### 2.2.1 Satellite-derived gridded products

Geophysical quantities of interest are derived from satellite observations, assimilated in physical models of varying complexity.

#### 2.2.1.1 Sea Surface Height

VarDyn is a variational mapping method jointly reconstructing Sea Surface Height (SSH) and Sea Surface Temperature (SST) ([Le Guillou et al., 2025](#)). The version used in our analysis assimilates both SWOT KaRin and Nadir altimeters data and produces daily  $0.05^\circ \times 0.05^\circ$  maps. This dataset provides both SSH and sea surface currents, derived from the SSH field using the cyclogeostrophic inversion method proposed by Bertrand, Le Sommer, et al. ([2025](#)) and implemented in the Python package `jxparrow` ([Bertrand, Vianna Zaia De Almeida, et al., 2025](#)).

#### 2.2.1.2 Sea Surface Wind

Wind acts both directly on the drifter (the leeway) and indirectly through its effect on waves and currents. We use the wind velocity at 10 meters above the surface from the  $0.125^\circ \times 0.125^\circ$  hourly ECMWF bias corrected

product ([WIND\\_GLO\\_PHY\\_L4\\_NRT\\_012\\_004, 2024](#)) developed by the Royal Netherlands Meteorological Institute.

### 2.2.1.3 Sea State

Waves also affect drifter trajectories through the Stokes drift. We employ the Stokes drift obtained by assimilating significant wave height in the wave model MFWAM, available in the  $0.083^\circ \times 0.083^\circ$  hourly Global Ocean Waves Analysis and Forecast product ([GLOBAL\\_ANALYSISFORECAST\\_WAV\\_001\\_027, 2023](#)) developed by Mercator Ocean International.

## 2.2 Drifter data

Starting from the raw GPS positions transmitted by the drifters, we perform several preprocessing steps before using them in our analysis.

### 2.2.2.1 L0 version

The L0 version of the data consists of datasets containing the original timestamps and positions (latitude and longitude) for each drifter, complemented by its deployment date and time. Each record also includes the time interval between successive measurements.

### 2.2.2.2 L1 version

The L1 version of the data is produced by applying the following Quality Control (QC) steps to the L0 dataset:

1. Spurious GPS locations were removed following the procedure described by Shane Elipot et al. ([2016](#)),
2. Curated trajectories were divided into segments whenever the time gap between two consecutive timestamps exceeded 6 hours,
3. Segments shorter than 1 day are discarded.

As shown in Table 1, these QC steps result in only a small reduction in the number of MELODI drifter observations. In contrast, about 20% of the SPOT observations were discarded, primarily due to transmission issues that caused large gaps in the original trajectories and consequently led to many short segments being removed.

Table 1: Number of observations and segments in L0 and L1 versions for SPOT and MELODI datasets.

Dataset	# Observations		# Segments	
	L0	L1	L0	L1
SPOT	24503	19846	20	189
MELODI	47399	46837	19	39

### 2.2.2.3 L2 version

Trajectories are resampled at a regular time interval of 1 hour using a linear interpolation for the positions and the velocities are then computed using central differences.

An example of L0, L1 and L2 trajectories for a SPOT drifter is shown in Figure 7. It can be seen that the L0 trajectory contains some spurious points, which are removed in the L1 and L2 versions. Holes in the L1 and L2 trajectories correspond to gaps larger than 6 hours in the original data. Holes are not filled by interpolation in the L2 version as those trajectories are then considered as distinct segments.

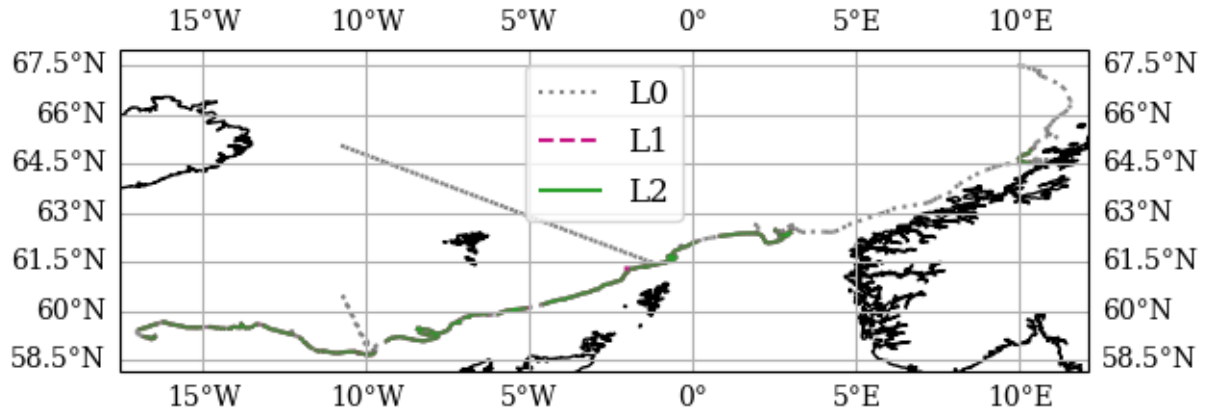


Figure 7: SPOT drifter 0-4498291 data (2025-05-12 – 2025-09-16) at different pre-processing levels.

Figure 8 presents the L2 trajectories of both SPOT and MELODI drifters deployed between Tromsø and Nice during OTC25.

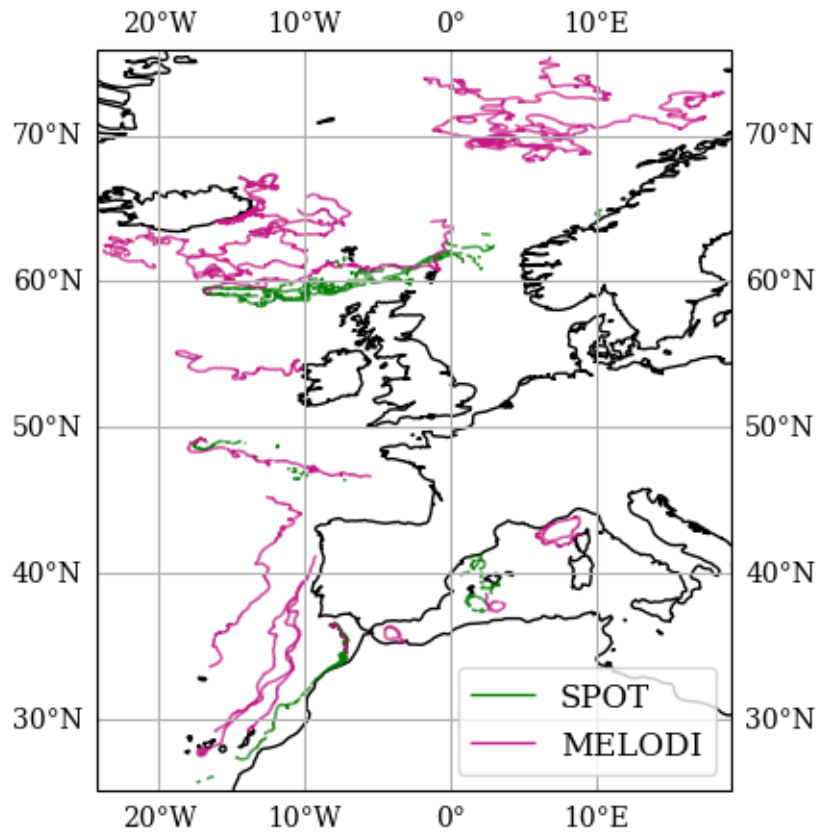


Figure 8: L2 drifters data from the OTC 25 (2025-04-25 – 2025-09-16).

## 2.3 Modeling of drifter trajectories

### 2.3.1 Linear combination

### 2.3.2 Maxey-Riley framework

The Maxey-Riley equations provide an accurate description of floating object drift, making them a useful model for predicting the trajectories of floaters in ocean environments. This framework takes into account all the forces that contribute to their horizontal movement: the *flow force* exerted on the particle by the fluid, the *added mass force* resulting from the displacement of part of the fluid with the particle, the *lift force*, which occurs when the particle rotates while moving in a (horizontal) shear flow, and the *drag force* due to the viscosity of the fluid. Here we present briefly the theory that leads to the Maxey-Riley framework, following (Beron-Vera et al., 2019). It is important to keep in mind that, despite its mathematical complexity, it is simply the result of applying Newton's second law:

$$m_p \ddot{x}_p = F_{\text{flow}} + F_{\text{mass}} + F_{\text{lift}} + F_{\text{drag}} \quad (1)$$

where  $m_p$  is the particle mass and  $\ddot{x}_p$  its acceleration.

Let us consider a spherical particle of radius  $a$  and density  $\rho$  floating in the interface between air and water. The *flow force* is given by

$$F_{\text{flow}} = \frac{m_f}{m_p} \frac{Dv_f}{Dt}, \quad (2)$$

where  $m_f$  is the mass of the displaced fluid,  $v_f$  is the fluid velocity and  $\frac{Dv_f}{Dt} = \frac{\partial v_f}{\partial t} + (\nabla v_f)v_f$  stands for material derivative.

The *added mass force* can be expressed as

$$F_{\text{mass}} = \frac{\frac{1}{2}m_f}{m_p} \left( \frac{Dv_f}{Dt} - \dot{v}_p \right), \quad (3)$$

where  $\dot{v}_p = \frac{\partial v_p}{\partial t}$  is the particle acceleration.

The *lift force*, generated by the particle rotation, reads:

$$F_{\text{lift}} = \frac{\frac{1}{2}m_f}{m_p} \omega_f (v_f - v_p)^\perp, \quad (4)$$

where  $\omega_f$  is the vertical vorticity of the fluid and the operator  $^\perp$  indicates a 90° counterclockwise rotation.

Finally, the *drag force* is given by

$$F_{\text{drag}} = \frac{12\mu_f A_f / l_f}{m_p} (v_f - v_p), \quad (5)$$

where  $\mu_f$  is the dynamic fluid viscosity,  $A_f = \pi a^2$  is the projected area of the particle and  $l_a = 2a$  is its projected length.

In order to adapt this fluid mechanics formulation to geophysical flows, a contribution from the Coriolis force is included in the flow and added mass force. The forces are averaged in the vertical direction over the particle's height, with the integration limits being from  $-h$  (immersed depth) to  $h_a$  (height above the surface), since the fluid variables take different values in the water region  $[-h, 0]$  and in the air region  $(0, h_a]$ . This process gives the explicit form of the Maxey-Riley framework:

$$\dot{v}_p + \left( f + \frac{1}{2} Ra \right) v_p^\perp + \tau^{-1} v_p = R \frac{Dv}{Dt} + R \left( f + \frac{1}{2} \omega \right) v^\perp + \tau^{-1} u, \quad (6)$$

where  $f$  is the Coriolis parameter,  $R$  is a parameter that depends on the depth  $h$  of the submerged spherical cap,  $\omega$  is the water vorticity, and  $\tau$  accounts for the inertial response time of the medium to the particle.  $u$  is defined as

$$u = (1 - \alpha)v + \alpha v_a \quad (7)$$

where  $v$  is the water velocity,  $v_a$  the air velocity and  $\alpha$  can be interpreted as a leeway factor. It should be noted that, contrarily to leeway models, where the wind parameter is chosen *ad hoc*, here  $\alpha$  is obtained from geometrical characteristics of the particle and it is not a fit parameter.

The drifters we deployed during the OTC25 campaign were not spheric. This difference is taken into account by a correction factor  $0 \leq \kappa \leq 1$  that changes the value of  $\tau$  and is defined as

$$\kappa^{-1} = \frac{1}{3} \frac{a_n}{a_v} + \frac{2}{3} \frac{a_s}{a_v}, \quad (8)$$

where  $a_n$ ,  $a_s$  and  $a_v$  are the radii of a sphere of the equivalent projected area, surface area and equivalent volume. For the case of a cylinder (like the MELODI drifter), they can be obtained as

$$a_n = \sqrt{\frac{2R_D H_D}{\pi}}, \quad a_s = R_D, \quad \text{and} \quad a_v = \sqrt[3]{\frac{3}{4} R_D^2 H_D}, \quad (9)$$

where  $R_D$  and  $H_D$  are the radius and the height of the cylindric drifter.

It has been shown that rotational effects from Earth are generally negligible when the floating object's dimensions are significantly smaller than approximately 1 km Wagner et al. (2022). We can thus neglect the Coriolis effect in our measurements, since our drifters are smaller than 30 cm.

We can do one last approximation under the assumption that the particle is small compared to the characteristic lengths of the flow (known as *slow manifold approximation*). In this case, the inertial response time is short and the Maxey-Riley framework can be simplified to:

$$\dot{x}_p = u + \tau u_\tau, \quad \text{with} \quad u_\tau = R + \frac{1}{3} R \omega v^\perp - \frac{Du}{Dt} - \frac{1}{3} R \omega u^\perp \quad (10)$$

where  $u$  is given by Equation 7. This framework is a two-dimensional system in  $x$  and does not require specification of the initial velocity for resolution. It is this equation the one we are going to resolve to model the trajectory of the drifters deployed during the campaign.

## 2.4 Pair dispersion

Spreading of a group of surface drifters can be characterized by the distance  $D$  between a pair of drifters and the relative diffusivity  $K$ , defined as:

$$K(D) = \frac{1}{2} \frac{\partial D^2}{\partial t}, \quad (11)$$

where  $t$  stands for the time (Van Sebille et al., 2015). Since we study the motion of floaters at the sea surface, we will use the 2-D Quasi-Geostrophic turbulence theory. add citations In this context, the dynamics of the pair separation can be classified in three regimes, depending on the scale of the underlying currents. There are two important length scales: the Rossby deformation radius, that is the distance at which rotational effects become important, and the scale of the eddies present in the flow.

For separations smaller than the Rossby deformation radius, we expect the pair dispersion  $D^2$  to increase exponentially with time and the pair diffusivity to be proportional to  $D^2$ . This is known as the “exponential regime”. If the separation is bigger than the Rossby deformation radius but smaller than the biggest eddies in the flow, the dynamics is known as “Richardson regime” and is expected to scale as  $D^2 \propto t^3$ . The pair diffusivity is expected to be  $K \propto D^{4/3}$ . These two regimes are *local*, meaning that their dynamics is governed by eddies of  $\mathcal{O}(D)$ . For scales larger than the eddies, i.e., for non-local dynamics, we expect a diffusive random walk regime with dispersion scaling linearly with time and  $K$  keeping a constant value. In this case, the diffusive character of the dynamics arises because each drifter of the pair is influenced by different, uncorrelated eddies.

We performed four deployments of five SPOT drifters each dedicated to study pair dispersion, as shown in Figure 3. The first deployment was performed on the 12th May on the Atlantic Sea, the second on the 18th May, the third on the 24th May just before crossing Gibraltar Strait, and one last deployment on May 30th at the mediterranean sea.

Source: [Instruments, data and methods](#)

## 3 Results

### 3.1 Modeling of drifter trajectories

#### 3.1.1 Maxey-Riley framework

We will use the data from MELODI drifters since they provide a better time resolution than the SPOT drifters (they transmit in regular intervals). As shown in Figure 2, they are not spherical. To take their shape into account, we calculate the radius of the sphere with equivalent projected area, surface area and equivalent volume (Equation 9), obtaining  $a_n = 0.08$  m,  $a_s = 0.12$  m and  $a_v = 0.11$  m. The weight on the bottom of the drifters is not taken into account for this calculations but the total weight of the drifter is considered to calculate its density. We use a combination of all the currents present at the surface to compute  $v_f$  (Eckman, Stokes and the cyclogesotrophic currents) and the wind at the surface to compute  $v_a$ .

We consider three representative cases: a deployment in the Norwegian Sea, one in the Atlantic Ocean and one in the Mediterranean Sea. Figure 9 shows the drifter real trajectory for a week after release in the Lofoten Vortex on the 24th April and the reconstructed trajectory from the Maxey-Riley framework, obtained using Equation 10. We can observe that the reconstructed trajectory follows the general tendency of the real one but it does not exactly follow the same path, and seems to move with a slower speed than the real drifter. It is worth noting that the drifter seems to be highly influenced by the wind (blowing northward).

Figure 10 shows the real and simulated trajectories for a deployment made in the Atlantic Ocean on the 23rd May. Remarkably, in this case the simulated trajectory is really close to the real one. Nevertheless, it does not seem to take into account the small scale oscillations visible in the real trajectory. These oscillations are usually generated by waves and are not visible in the sattelite data, which could explain why the simulation did not account for them.

It is important to remind that these numerical resolutions do not have any fitting parameter. They only depend on the currents and wind fields (products derived from sattelite data), the initial position of the drifter and its geometry. The numerical resolution is thus very sensitive to changes in those parameters. For example, several runs of the simulation with slight changes of the initial position give rise to a different outcome, which may not be close to the real one. Figure 11 shows the real and simulated trajectories for a deployment made in the Mediterranean Sea on the 30th May. In this case, the deployment was made at the interface between two vortices and the wind was blowing westward. The simulated trajectory does not follow the real one. We will discuss the possible reasons in the Section 4.

### 3.2 Pair dispersion

We used the home-made SPOT drifters to study pair dispersion. They are designed to transmit their position every 30 minutes. However, this is not always the case. In order to calculate the distance betwen a pair of

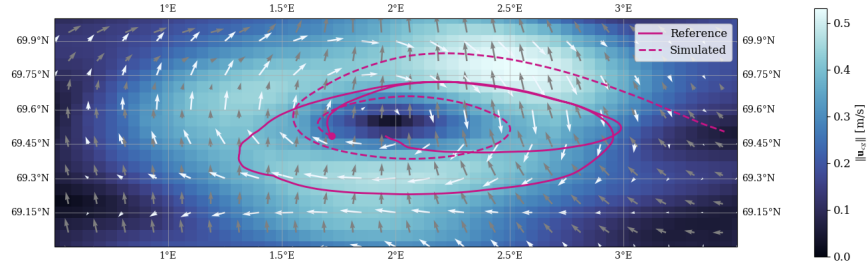


Figure 9: Drifter trajectory on the Lofoten Vortex during one week after deployment. The solid lines indicate the real trajectory, while the dashed lines show the result of solving the Maxey-Riley set. The colors indicate the absolute value of the cyclogeostrophic current at the moment of release. The white arrows show the direction of the current and the gray arrows indicate the wind direction.

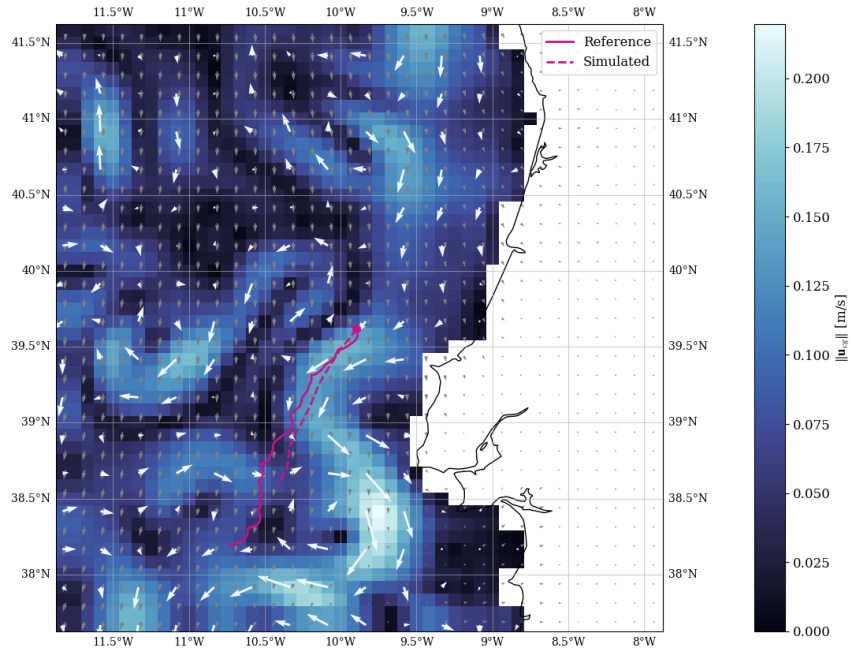


Figure 10: Drifter trajectory in the Atlantic Ocean, near the Portuguese coast, during one week after deployment. The solid lines indicate the real trajectory, while the dashed lines show the result of solving the Maxey-Riley set. The colors indicate the absolute value of the cyclogeostrophic current at the moment of release. The white arrows show the direction of the current and the gray arrows indicate the wind direction.

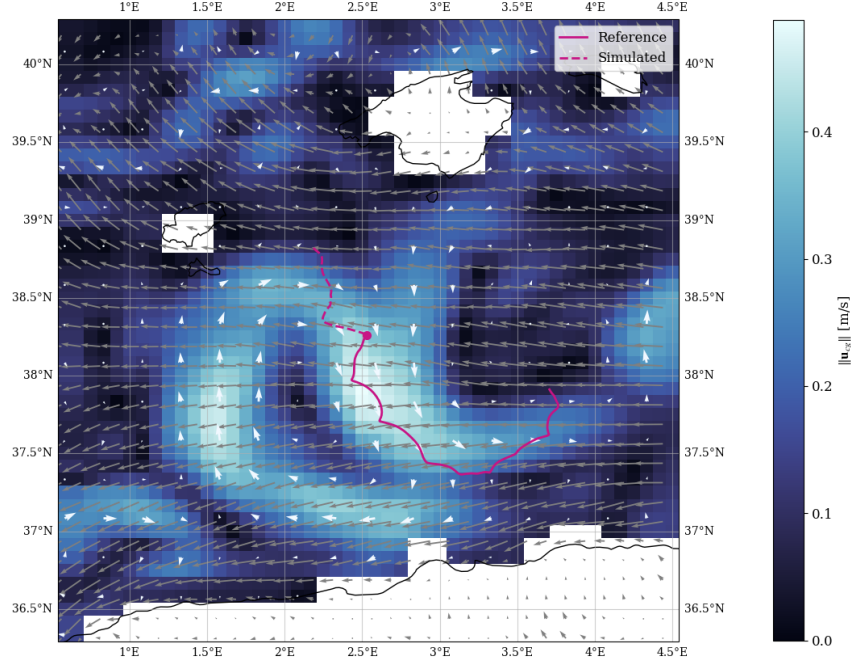


Figure 11: Drifter trajectory on the Mediterranean Sea during one week after deployment. The solid lines indicate the real trajectory, while the dashed lines show the result of solving the Maxey-Riley set. The colors indicate the absolute value of the cyclogeostrophic current at the moment of release. The white arrows show the direction of the current and the gray arrows indicate the wind direction.

drifters, they should have transmitted in the same time interval. Figure 12 shows in black when each drifter transmitted its position, using a time interval of 30 minutes. This trajectories have already been interpolated in time (L2 version). For each deployment of  $N = 5$  drifters, there are  $N(N - 1)/2 = 10$  pairs. For each pair, we will consider their positions if they transmitted at the same time interval.

Considering the variability of the conditions for making *in-situ* measurements, each group of drifters behave differently. We can observe that there are several pairs for the first and third deployments, but less simultaneous transmissions for the second and fourth. For example, on the last deployment one drifter stop transmitting almost immediately, so we have only 6 pairs. But if we take a closer look at Figure 12 (d) we see that in practice we have only one pair of drifters that transmitted for more than a month.

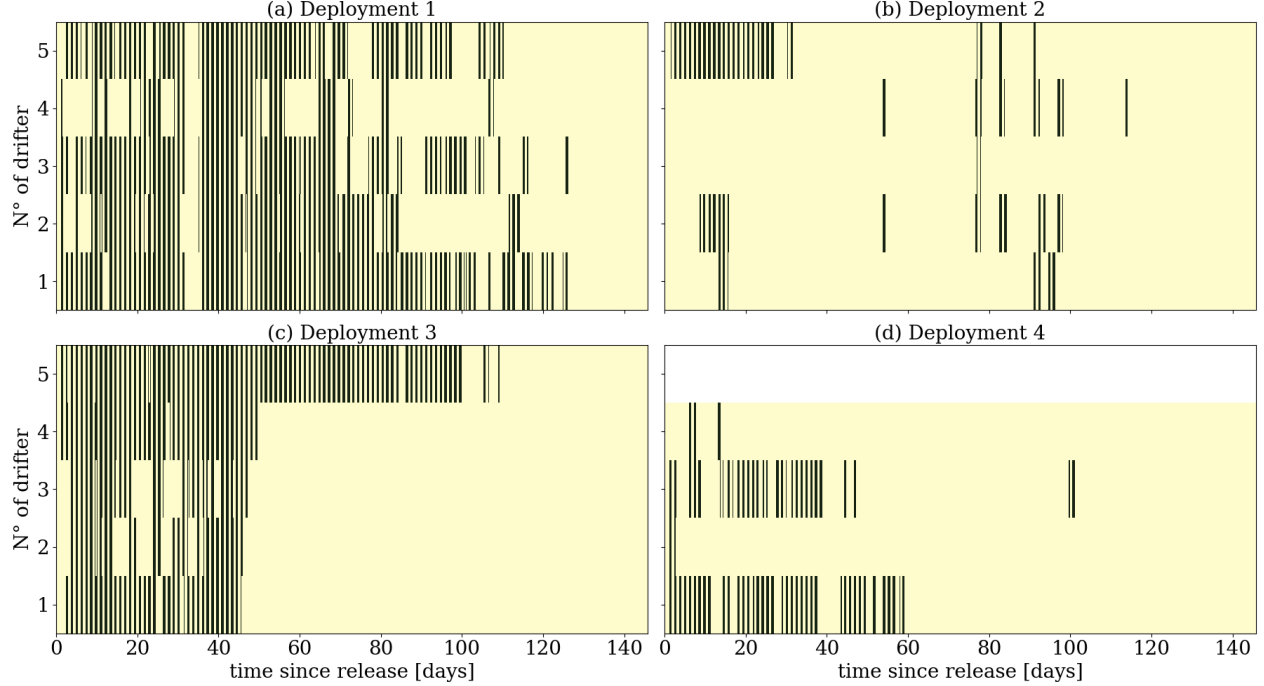


Figure 12: Mask showing if the drifters transmitted their position. The black rectangles indicate that the transmission was successful, yellow rectangles indicate that they did not transmit. L2 trajectories are used for the analysis.

Figure 13 shows the pair dispersion  $D^2$  as a function of time for each deployment. As discussed before, for the first and third deployments we have several pairs while we do not have enough data for the second and fourth. In Figure 13 (a) we can clearly observe two different behaviors: an exponential growth for the first two weeks after release, and a different regime after. Pink lines indicate the exponential and the Richardson regimes, showing a good agreement with the measured data. The third deployment, however, seems to show only an exponential behavior. It follows a scaling law  $D^2 \propto e^{\alpha t}$ , with a growth rate of  $\alpha = 5$ . Unexpectedly, this growth rate is bigger than the one of the first deployment but the particles remain in an exponential regime. This can be due to a difference in transition thresholds. If the transition scale (the size of the biggest eddies in the flow) varies, we expect the first group of drifters to reach the Richardson regime sooner despite slower growth, while the third group of drifters remain in exponential regime but still relatively close together, not yet having reached their larger transition threshold.

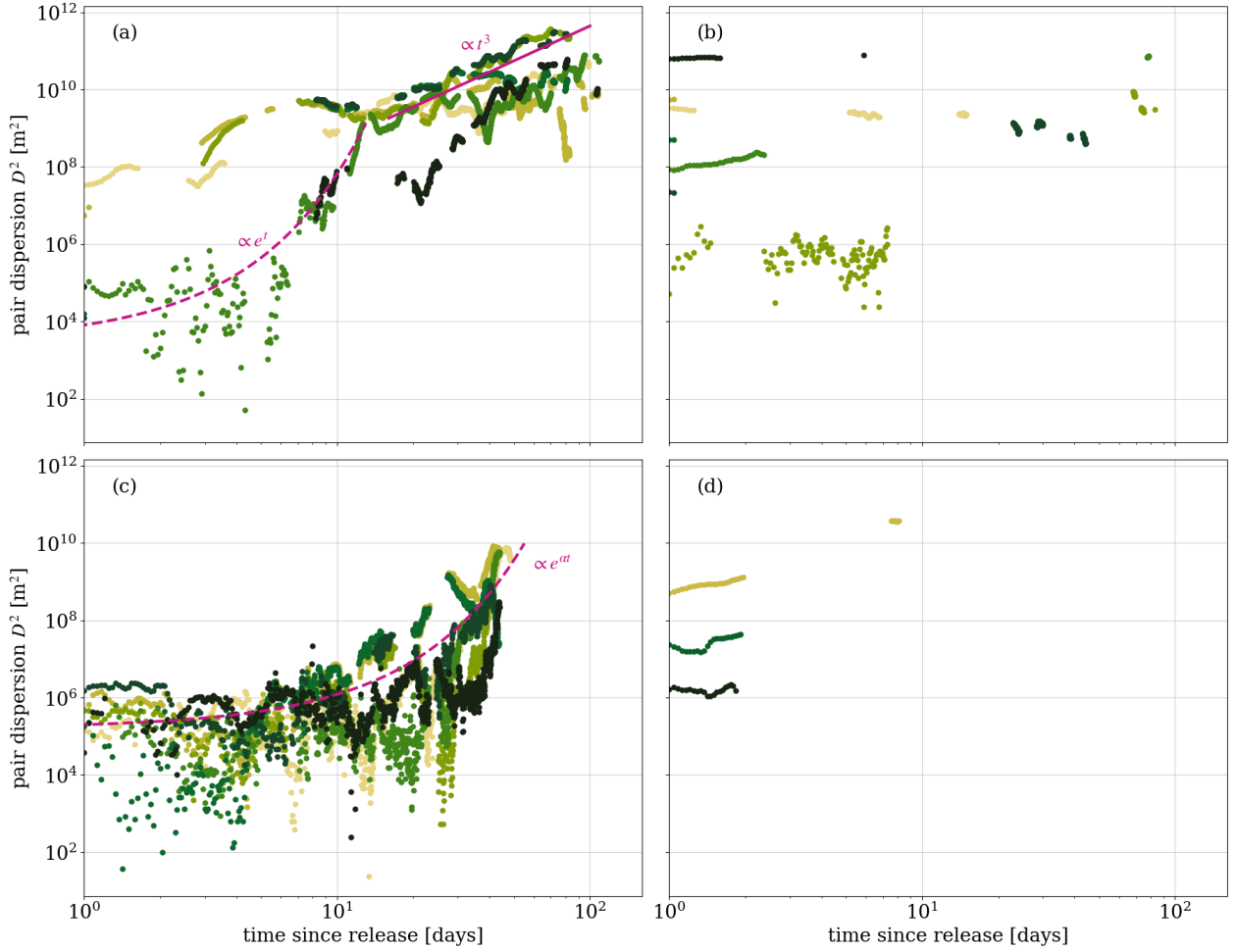


Figure 13: Pair dispersion for each deployment as a function of the time since release. The colors represent the different pairs. The pink dashed line shows the scaling corresponding to the exponential regime and the solid pink line represents the scaling of the richardson regime.

The rate of change of separation, or pair diffusivity, has been calculated using Equation 11 and is shown in Figure 14. Both regimes are shown for all deployments. For the first one, it does not seem to be so clear that there are two regimes, as it was in Figure 13 (a). The third one, however, shows one clear tendency where  $K \propto D^2$ . The second and fourth deployment do not have enough data to determine the regime that governs its dynamics.

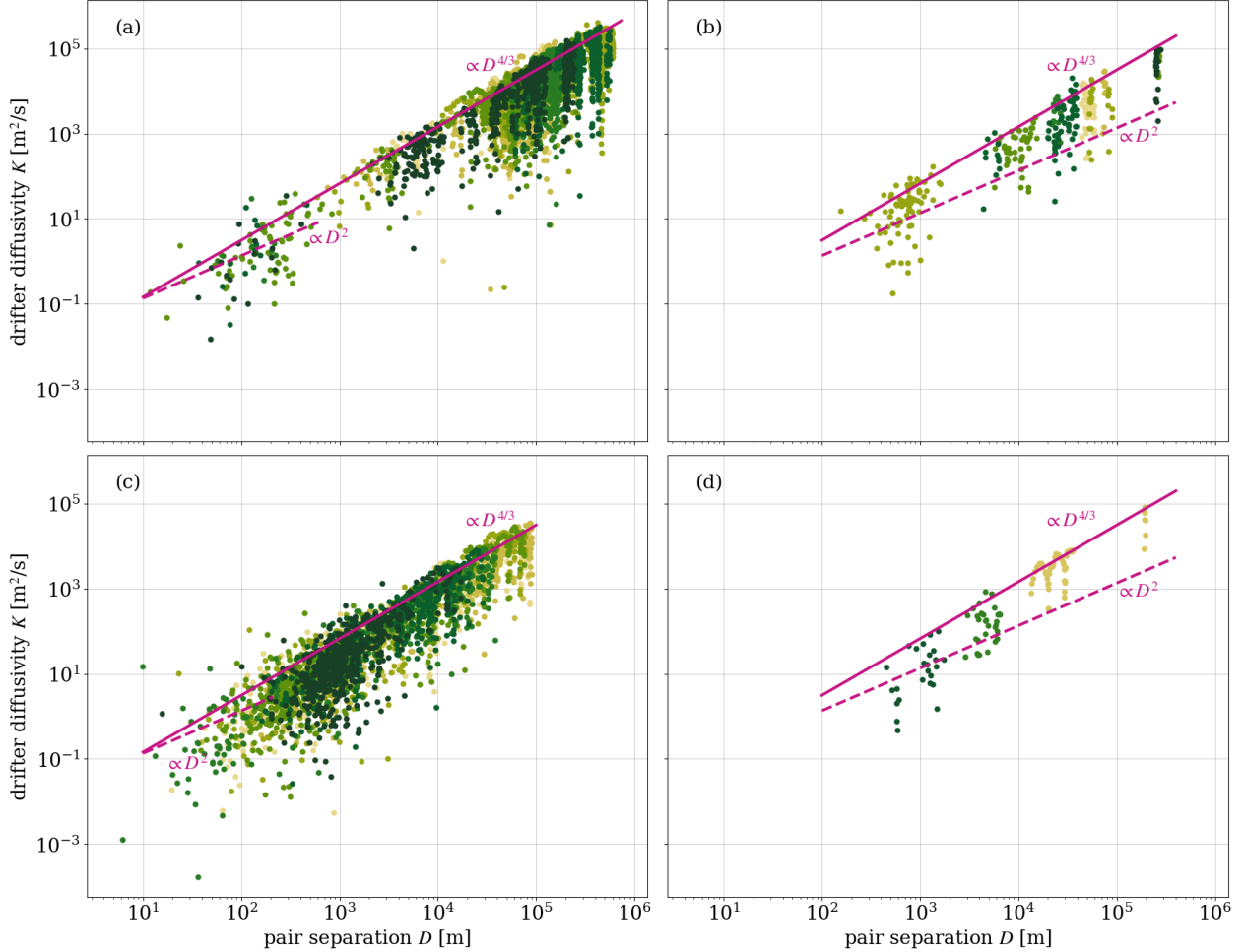


Figure 14: Pair diffusivity as a function of the distance between pairs. The colors represent the different pairs. The pink dashed line shows the scaling corresponding to the exponential regime and the solid pink line represents the scaling of the richardson regime.

Source: [Results](#)

## 4 Discussion

### 4.1 Modeling of drifter trajectories

#### 4.1.1 Maxey-Riley framework

Surprisingly, the Maxey-Riley framework has been used only once to describe the dynamics of floating particles in the ocean (Olascoaga et al., 2020). Yet it is the theory derived from first principles that accounts for the forces exerted on a floating particle at the interface between a fluid and air. Unlike most theories that describe particle motion in the ocean, this model does not have fitting parameters. One typical fitting parameter in studies on search and rescue (Breivik & Allen, 2008) is the leeway coefficient, that accounts for windage effects. In the framework of Equation 10, the parameters  $\alpha$ ,  $R$  and  $\tau$  are calculated based on the particle geometry and the properties of the objects and the fields (density, viscosity).

Passing from the full Maxey-Riley equations (Equation 6) to the slow manifold approximation (Equation 10) facilitates numerical resolution since we passed from a second order differential equation (that is, two ordinary differential equations with two initial conditions) to a first order differential equation. We only need the initial

position of the drifter but not its initial velocity. Taking a look at Figure 11 we could think that the slow manifold approximation may have been an overstatement. However, the only assumption there is that the drifter size is smaller than the characteristic lengths present in the system, which remains true. Let us review which assumptions we made may modify significantly the behavior of the numerical simulations.

First, we can wonder if the parameter  $\alpha$ , equivalent to a leeway coefficient, is well determined, since the wind seems to have an important effect on the obtained trajectories. We obtained a value of  $\alpha = 1\%$ , slightly smaller than the typical 3% commonly used as a leeway coefficient. We thus conclude that the mismatch between the trajectories must come from somewhere else.

MELODI drifters are not spheres, but are not perfect cylinders either. The correction  $\kappa$  (Equation 8) that accounts for the deviation from a sphere is not exactly well calculated because it is not straightforward to determine the radii of the equivalent sphere taking into account the metallic anchor included in the MELODI drifters. This discrepancy could be a source of error, because we are not only obtaining  $\kappa$  from these values but also the density of the drifters. When more data from other drifters becomes available, we will compare our results to drifters with different geometries.

Another possible source of error is the spatial and temporal resolution of satellite data. To accurately compute a numerical resolution of Equation 10, we need a short temporal step (for example, one minute). But the satellite data is not available in such short periods and it is thus interpolated. A similar mechanism occurs with the spatial data. Satellites do not retrieve information on the small scales that affect the drifter movement. The Maxey-Riley framework assumes that we know the fields in the scales we need them but this is not the case. We think this is the biggest source of discrepancy between the real trajectories and the simulated ones. Nevertheless, the Maxey-Riley set provides a remarkably accurate description using only the initial position, and we are still working on exploiting its potential to understand the dynamics of floating objects in the ocean.

## 4.2 Pair dispersion

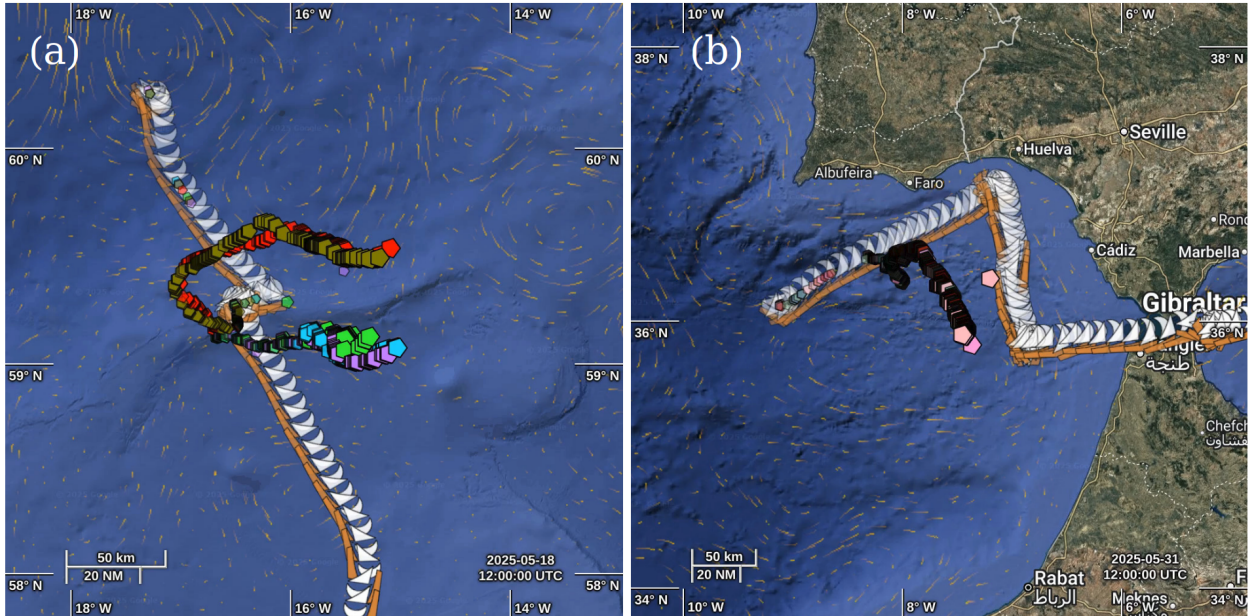


Figure 15: Seashots taken from OVL OceanDataLab, showing the trajectory of the Statsraad Lehmkuhl, the cyclogesotrophic current (from Vardyn) and the position of the SPOT drifters over two weeks, starting the day of the deployment for (a) the first deployment and (b) the third one.

From the data from the first deployment, we could distinguish two different regimes (see Figure 13). However, the separation between them was not clear on the pair diffusivity (Figure 14). The change of regime arrives at

approximately two weeks after the deployment, when the distance between pairs is around 70 km. Figure 15 shows the position of the ship, the drifters and the cyclogesotrophic current from the release until this moment. In the panel (a) we can see the seashot corresponding to the first deployment. We can observe that the distance  $D$  is of the order of the eddies, but not yet the biggest eddies present in the flow. It makes sense that, in this case, the dynamics is still local but changes from a regime where they have been in the same eddy to an intermediate one. At the moment of the writing, five months after the release, the system did not reach yet the diffusive regime.

Regarding the third deployment, we can interpret the results shown in the previous section by looking at Figure 15. Two weeks after the deployment, the drifters move still all together and the distance they travelled is much smaller than the eddies present in the flow. It is expected, in this case, that the system remains in a local regime for longer. Our observations are in agreement with the previous results from the literature (Van Sebille et al., 2015) (Röhrs et al., 2023), including the specific two week interval before the transition between regimes in the North Sea (Meyerjürgens et al., 2020).

Source: [Discussion](#)

## 5 Conclusion

During the campaign, we deployed 43 drifters of five different types and successfully modelled their trajectories using two independent approaches. Both methods reveal that drifter motion is governed by small-scale currents that remain poorly resolved in satellite observations. We demonstrate that these unresolved currents can be recovered along individual trajectories through an optimization procedure within the Linear Combination method. To establish a predictive framework, we implement the Maxey-Riley formulation, which accurately captures the observed dynamics in the majority of cases.

Additionally, we analyzed relative pair dispersion for drifter groups of identical type. Our results show an initial exponential growth phase transitioning to Richardson-regime scaling behavior, consistent with established theoretical predictions and previous observational studies. This work is ongoing, and further analysis will be conducted once the remaining drifter trajectories are recovered.

## 6 Acknowledgements



We want to thank ESA for giving us the opportunity to participate in the Ocean Training Course 2025. We thank Craig Donlon, Fabrice Collard and Johnny Johannessen for organizing the campaign. We thank Alexey Mironov for technical help with the drifters. We thank everyone that helped us deploy and follow the drifters. We thank the amazing group of people we had the honour to work and live with.

- Beron-Vera, F., Olascoaga, M., & Miron, P. (2019). Building a maxey–riley framework for surface ocean inertial particle dynamics. *Physics of Fluids*, 31(9).
- Bertrand, V., Le Sommer, J., Vianna Zaia De Almeida, V., Samson, A., & Cosme, E. (2025). A Robust Variational Framework for Cyclogesotrophic Ocean Surface Current Retrieval. *EGUsphere*, 1–22. <https://doi.org/10.5194/egusphere-2025-4172>

- Bertrand, V., Vianna Zaia De Almeida, V., Le Sommer, J., & Cosme, E. (2025). Jaxparrow. Zenodo. <https://doi.org/10.5281/zenodo.14871648>
- Breivik, Ø., & Allen, A. A. (2008). An operational search and rescue model for the norwegian sea and the north sea. *Journal of Marine Systems*, 69(1-2), 99–113.
- Calvert, Ross, McAllister, M., Whittaker, C., Raby, A., Borthwick, A., & Van Den Bremer, T. (2021). A mechanism for the increased wave-induced drift of floating marine litter. *Journal of Fluid Mechanics*, 915, A73.
- Calvert, R., Peytavin, A., Pham, Y., Duhamel, A., Zanden, J. van der, Essen, S. van, et al. (2024). A laboratory study of the effects of size, density, and shape on the wave-induced transport of floating marine litter. *Journal of Geophysical Research: Oceans*, 129(7), e2023JC020661.
- Christensen, K. H., Breivik, Ø., Dagestad, K.-F., Röhrs, J., & Ward, B. (2018). Short-term predictions of oceanic drift. *Oceanography*, 31(3), 59–67.
- Clark, L. K., DiBenedetto, M. H., Ouellette, N. T., & Koseff, J. R. (2020). Settling of inertial nonspherical particles in wavy flow. *Physical Review Fluids*, 5(12), 124301.
- DiBenedetto, M. H., Clark, L. K., & Pujara, N. (2022). Enhanced settling and dispersion of inertial particles in surface waves. *Journal of Fluid Mechanics*, 936, A38.
- Elipot, Shane, Lumpkin, R., Perez, R. C., Lilly, J. M., Early, J. J., & Sykulski, A. M. (2016). A global surface drifter data set at hourly resolution. *Journal of Geophysical Research: Oceans*, 121(5). <https://doi.org/10.1002/2016JC011716>
- Elipot, S., Lumpkin, R., Perez, R. C., Lilly, J., Early, J., & Sykulski, A. (2016). A global surface drifter data set at hourly resolution. *Journal of Geophysical Research: Oceans*, 121(5), 2937–2966.
- GLOBAL\_ANALYSISFORECAST\_WAV\_001\_027. (2023). Global ocean waves analysis and forecast [Data set]. E.U. Copernicus Marine Service Information (CMEMS). Marine Data Store (MDS). <https://doi.org/10.48670/moi-00017>
- Le Guillou, F., Chapron, B., & Rio, M.-H. (2025). VarDyn: Dynamical Joint-Reconstructions of Sea Surface Height and Temperature From Multi-Sensor Satellite Observations. *Journal of Advances in Modeling Earth Systems*, 17(4), e2024MS004689. <https://doi.org/10.1029/2024MS004689>
- Maxey, M. R., & Riley, J. J. (1983). Equation of motion for a small rigid sphere in a nonuniform flow. *The Physics of Fluids*, 26(4), 883–889.
- MELODI. (2024). Retrieved from <https://www.eodyn.com/melodi-2/>
- Meyerjürgens, J., Ricker, M., Schakau, V., Badewien, T. H., & Stanev, E. V. (2020). Relative dispersion of surface drifters in the north sea: The effect of tides on mesoscale diffusivity. *Journal of Geophysical Research: Oceans*, 125(8), e2019JC015925.
- Olascoaga, M., Beron-Vera, F., Miron, P., Triñanes, J., Putman, N., & Lumpkin, G. J., R .and Goni. (2020). Observation and quantification of inertial effects on the drift of floating objects at the ocean surface. *Physics of Fluids*, 32(2).
- Quilfen, Y., & Chapron, B. (2019). Ocean surface wave-current signatures from satellite altimeter measurements. *Geophysical Research Letters*, 46(1), 253–261.
- Röhrs, J., Sutherland, G., Jeans, G., Bedington, M., Sperrevik, A. K., Dagestad, K.-F., et al. (2023). Surface currents in operational oceanography: Key applications, mechanisms, and methods. *Journal of Operational Oceanography*, 16(1), 60–88.
- SPOT. (2024). Retrieved from <https://github.com/vadmbertr/otc25-cannelloni>
- Sutherland, B. R., DiBenedetto, M., Kaminski, A., & Van Den Bremer, T. (2023). Fluid dynamics challenges in predicting plastic pollution transport in the ocean: A perspective. *Physical Review Fluids*, 8(7), 070701.
- Van Sebille, E., Waterman, S., Barthel, A., Lumpkin, R., Keating, S. R., Fogwill, C., & Turney, C. (2015). Pairwise surface drifter separation in the western pacific sector of the southern ocean. *Journal of Geophysical Research: Oceans*, 120(10), 6769–6781.
- Van Sebille, E., Aliani, S., Law, K. L., Maximenko, N., Alsina, J. M., Bagaev, A., et al. (2020). The physical oceanography of the transport of floating marine debris. *Environmental Research Letters*, 15(2), 023003.
- Wagner, T. J., Eisenman, I., Ceroli, A. M., & Constantinou, N. C. (2022). How winds and ocean currents influence the drift of floating objects. *Journal of Physical Oceanography*, 52(5), 907–916.
- WIND\_GLO\_PHY\_L4\_NRT\_012\_004. (2024). Global ocean hourly sea surface wind and stress from scatterometer and model [Data set]. E.U. Copernicus Marine Service Information (CMEMS). Marine Data Store (MDS). <https://doi.org/10.48670/moi-00305>